We are IntechOpen,
the world's leading publisher of
Open Access books
Built by scientists, for scientists

4,800
Open access books available

122,000
International authors and editors

135M
Downloads

Our authors are among the

154
Countries delivered to

TOP 1%
most cited scientists

12.2%
Contributors from top 500 universities

CLARIVATE ANALYTICS

BOOK CITATION INDEX

INDEXED

WEB OF SCIENCE™

Selection of our books indexed in the Book Citation Index
in Web of Science™ Core Collection (BKCI)

Interested in publishing with us?
Contact book.department@intechopen.com

Numbers displayed above are based on latest data collected.
For more information visit www.intechopen.com

Active Fault Diagnosis and Major Actuator Failure Accommodation: Application to a UAV

François Bateman[1], Hassan Noura[2] and Mustapha Ouladsine[3]
[1]*French Air Force Academy, Salon de Provence*
[2]*United Arab Emirates University, Al-Ain*
[3]*Paul Cezanne University, Marseille*
[1,3]*France*
[2]*United Arab Emirates*

1. Introduction

Interest in Unmanned Aerial Vehicles (UAVs) is growing worldwide. Nevertheless there are numerous issues that must be overcome as a precondition to their routine and safe integration in military and civilian airspaces. Chief among these are absence of certification standards and regulations addressing UAV systems, poor reliability record of UAV systems and operations. Standards and regulations for airworthiness certification and flight operations in the military and civilian airspaces are being studied (Brigaud, 2006). In this respect, the USAR standard suggests a mishap rate of one catastrophic mishap per one million hours (Brigaud, 2006). To reach such performances, upcoming technologies have the promise of significantly improving the reliability of UAVs.

In this connection, a detailed study (OSD, 2003) shows that most of the breakdowns are due to system failures such as propulsion, data link and Flight Control Systems (FCS). These latter include all systems contributing to the aircraft stability and control such as avionics, air data system, servo-actuators, control surfaces/servos, on-board software, navigation, and other related subsystems. As regards FCS, it is recommended in (OSD, 2003) to incorporate emerging technologies such as Self-Repairing Flight Control Systems (SRFCS) which have the capability to diagnose and to repair malfunctions.

In this respect, Fault-tolerant control (FTC) are control systems that have the ability to accommodate failures automatically in order to maintain system stability and a sufficient level of performance. FTC are classified into passive and active methods. The analytical fault-tolerant control operation can be achieved passively by the use of a control law designed to guarantee an acceptable degree of performance in fault-free case and to be insensitive to some faults. However, the passive methods are unsuitable to deal with a significant number of faults. In particular, for an aircraft, it may be tricky to design an *a priori* controller able to accommodate the whole of the faults affecting the control surfaces. By contrast, an active FTC consists of adjusting the controllers on-line according to the fault magnitude and type, in order to maintain the closed-loop performance of the system. To do so, a fault detection and isolation (FDI) module which provides information about the fault is required (Noura et al., 2009). Active FTC mechanisms may be implemented either via pre-computed control laws or via on-line automatic redesign.

In this respect, FDI and FTC applied to aeronautical systems have received considerable attention in the literature. However, regarding the control surface failures, some problematics tackled in this chapter are underlined:

- severe failures are considered and the control surfaces may abruptly lock in any position in their deflection range,

- each control surface being indenpendently driven, an actuator failure produces aerodynamical couplings between the longitudinal and the lateral axis,

- the UAV is equipped with an autopilot which masks the failure effects,

- the aircraft studied is a small UAV and the control surface positions are not measured, which makes the fault detection difficult,

- the control surfaces have redundant effects, which complicates the fault isolation,

- the FTC must take into account the bounds existing on the control surface deflections and the flight envelope.

In this chapter, a nonlinear UAV model which allows to simulate assymetrical control surface failures is presented (Bateman et al., 2009). In fault-free mode, a nominal control law based on an Eigenstructure Assignment (EA) strategy is designed. As the control surface positions are not measured, a diagnosis system is performed with a bank of observers able to estimate the unkown inputs. However, as the two ailerons offert redundant effects, isolating a fault on these actuators requires an active diagnosis method (Bateman et al., 2008a). In the last part, a precomputed FTC strategy dedicated to accommodate for a ruddervator failure is depicted (Bateman et al., 2008b).

All the models can be simulated with MATLAB-SIMULINK. Files and tutorial can be downloaded at http://www.lsis.org/bateman/UAV.zip.

2. Aircraft model

The aircraft studied in this paper and shown in Fig.1 is an inverted V-tail UAV. It is assumed that its controls are fully indenpendent: δ_x is the throttle, δ_{ar}, δ_{al}, δ_{fr}, δ_{fl}, δ_{er}, δ_{el} control the right and left ailerons, the right and left flaps, the right and left inverted V tail control surfaces respectively. These latter controls are named ruddervators because they combine the tasks of the elevators and rudder. In the fault-free mode, the ailerons and the ruddervators are known as the primary control surfaces, they produce the roll, the pitch and the yaw. As far as the flaps are concerned, in the fault-free mode, they are only used to produce a lift increment during takeoff and a drag increment during landing. They are known as the secondary control surfaces.

It is assumed that each one of the primary control surfaces may lock at any arbitrary position on its deflection range. To compensate for the fault, the FTC exploits the redundancies provided by the remaining control surfaces. In this pespective, the UAV model has to consider the aerodynamic effects produced by each control surface.

The following dynamic model of the aircraft is presented in the case of a rigid-body aircraft, the weight m is constant and the centre of gravity $c.g.$ is fixed position. Let $R_E = (O, \mathbf{x_E}, \mathbf{y_E}, \mathbf{z_E})$ be a right-hand inertial frame such that $\mathbf{z_E}$ is the vertical direction downwards the earth, $\boldsymbol{\xi} = (x, y, z)$ denotes the position of $c.g.$ in R_E. Let $R_b = (c.g., \mathbf{x_b}, \mathbf{y_b}, \mathbf{z_b})$ be a right-hand body fixed frame for the UAV, at $t = 0$ R_E and R_b coincide. The linear velocities $\boldsymbol{\mu} = (u, v, w)$ and the angular velocities $\boldsymbol{\Omega} = (p, q, r)$ are expressed in the body frame R_b where p, q, r are roll, pitch and yaw respectively. The orientation of the rigid body in R_E is located with the bank angle

Fig. 1. The RQ7A Shadow 200 UAV

ϕ, the pitch angle θ and the heading angle ψ. The transformation from R_b to R_E is given by a transformation matrix $\mathbf{T_{bE}}$:

$$\mathbf{T}_{bE} = \begin{pmatrix} \cos\theta\cos\psi & \sin\phi\sin\theta\cos\psi - \cos\phi\sin\psi & \cos\phi\sin\theta\cos\psi + \sin\phi\sin\psi \\ \cos\theta\sin\psi & \sin\phi\sin\theta\sin\psi + \cos\phi\cos\psi & \cos\phi\sin\theta\sin\psi - \sin\phi\cos\psi \\ -\sin\theta & \sin\phi\cos\theta & \cos\phi\cos\theta \end{pmatrix} \tag{1}$$

Forces $F_x^{R_b}, F_y^{R_b}, F_z^{R_b}$ acting on the aircraft are expressed in R_b, they originate in gravity $\mathbf{F_{grav}}$, propulsion $\mathbf{F_{prop}}$, and aerodynamic effects $\mathbf{F_{aero}}$. According to Newton's second law:

$$\begin{pmatrix} \dot{u} \\ \dot{v} \\ \dot{w} \end{pmatrix} = \frac{1}{m} \begin{pmatrix} F_x^{R_b} \\ F_y^{R_b} \\ F_z^{R_b} \end{pmatrix} - \begin{pmatrix} p \\ q \\ r \end{pmatrix} \wedge \begin{pmatrix} u \\ v \\ w \end{pmatrix} \tag{2}$$

where $\wedge$ denotes the cross product. Let $R_w = (c.g., \mathbf{x_w, y_w, z_w})$ be the wind reference frame where $\mathbf{x_w}$ is aligned with the true airspeed V. The orientation of the body reference frame in the wind reference frame is located with the angle of attack α and the sideslip β. The transformation from R_b to R_w is given by a transformation matrix $\mathbf{T_{bw}}$:

$$\mathbf{T}_{bw} = \begin{pmatrix} \cos\alpha\cos\beta & \sin\beta & \sin\alpha\cos\beta \\ -\cos\alpha\sin\beta & \cos\beta & -\sin\alpha\sin\beta \\ -\sin\alpha & 0 & \cos\alpha \end{pmatrix} \tag{3}$$

Furthermore, the aerodynamic state variables (V, α, β) and their time derivatives can be formulated using $\mathbf{T_{bw}}$ from $\boldsymbol{\mu}$ (Rauw, 1993).

$$\begin{aligned} V &= \sqrt{u^2 + v^2 + w^2} \\ \alpha &= \arctan\left(\frac{w}{u}\right) \\ \beta &= \arctan\left(\frac{v}{\sqrt{u^2 + w^2}}\right) \end{aligned} \tag{4}$$

For the sake of clarity, the forces are written in the reference frame where their expressions are the simplest. They are transformed into the desired frame by means of the matrices $\mathbf{T_{bE}}$ and

$\mathbf{T_{bw}}$ or their inverse.

$$\mathbf{F_{grav}}^{R_E} = \begin{pmatrix} 0 & 0 & g \end{pmatrix}^T$$

$$\mathbf{F_{prop}}^{R_b} = \left(\frac{k\rho(z)}{V}\delta_x \ 0 \ 0 \right)^T \tag{5}$$

$$\mathbf{F_{aero}}^{R_w} = \bar{q}S \begin{pmatrix} -C_D & C_y & -C_L \end{pmatrix}^T$$

The model of the engine propeller is given in (Boiffier, 1998), ρ is the air density, k is a constant characteristic of the propeller engine, $\bar{q} = \frac{1}{2}\rho V^2$ and S denote the aerodynamic pressure and a reference surface. The aerodynamic force coefficients are expressed as linear combination of the state elements and control inputs. The values of these aerodynamic coefficients can be found in the attached MATLAB files.

$$C_D = C_{D0} + \frac{S}{\pi b^2}C_L^2 + C_{D\delta_{ar}}|\delta_{ar}| + C_{D\delta_{al}}|\delta_{al}| + C_{D\delta_{fr}}|\delta_{fr}| + C_{D\delta_{fl}}|\delta_{fl}| + C_{D\delta_{er}}|\delta_{er}| + C_{D\delta_{el}}|\delta_{el}|$$

$$C_y = C_{y\beta}\beta + C_{y\delta_{ar}}\delta_{ar} + C_{y\delta_{al}}\delta_{al} + C_{y\delta_{fr}}\delta_{fr} + C_{y\delta_{fl}}\delta_{fl} + C_{y\delta_{er}}\delta_{er} + C_{y\delta_{el}}\delta_{el} \tag{6}$$

$$C_L = C_{L0} + C_{L\alpha}\alpha + C_{L\delta_{ar}}\delta_{ar} + C_{L\delta_{al}}\delta_{al} + C_{L\delta_{fr}}\delta_{fr} + C_{L\delta_{fl}}\delta_{fl} + C_{L\delta_{er}}\delta_{er} + C_{L\delta_{el}}\delta_{el}$$

The relationships between the angular velocities, their derivatives and the moments $\mathcal{M}_x^{R_b}$, $\mathcal{M}_y^{R_b}$, $\mathcal{M}_z^{R_b}$ applied to the aircraft originate from the general moment equation. $\mathbf{J}$ is the inertia matrix.

$$\begin{pmatrix} \dot{p} \\ \dot{q} \\ \dot{r} \end{pmatrix} = \mathbf{J}^{-1}\left[\begin{pmatrix} \mathcal{M}_x^{R_b} \\ \mathcal{M}_y^{R_b} \\ \mathcal{M}_z^{R_b} \end{pmatrix} - \begin{pmatrix} p \\ q \\ r \end{pmatrix} \wedge \mathbf{J}\begin{pmatrix} p \\ q \\ r \end{pmatrix} \right] \tag{7}$$

The moments are expressed in R_b, they are due to aerodynamic effects and are modeled as follows:

$$\left(\mathcal{M}_x^{R_b} \ \mathcal{M}_y^{R_b} \ \mathcal{M}_z^{R_b} \right) = \bar{q}S \begin{pmatrix} bC_l & \bar{c}C_m & bC_n \end{pmatrix} \tag{8}$$

where $\bar{c}$ and b are the mean aerodynamic chord and the wing span. The aerodynamic moment coefficients are expressed as a linear combination of state elements and control inputs as

$$C_l = C_{l\beta}\beta + C_{lp}\frac{bp}{2V} + C_{lr}\frac{br}{2V} + C_{l\delta_{ar}}\delta_{ar} + C_{l\delta_{al}}\delta_{al} + C_{l\delta_{er}}\delta_{er} + C_{l\delta_{el}}\delta_{el} + C_{l\delta_{fr}}\delta_{fr} + C_{l\delta_{fl}}\delta_{fl} \tag{9}$$

$$C_m = C_{m0} + C_{m\alpha}\alpha + C_{mq}\frac{\bar{c}q}{2V} + C_{m\delta_{ar}}\delta_{ar} + C_{m\delta_{al}}\delta_{al} + C_{m\delta_{er}}\delta_{er} + C_{m\delta_{el}}\delta_{el} + C_{m\delta_{fr}}\delta_{fr} + C_{m\delta_{fl}}\delta_{fl}$$

$$C_n = C_{n\beta}\beta + C_{np}\frac{bp}{2V} + C_{nr}\frac{br}{2V} + C_{n\delta_{ar}}\delta_{ar} + C_{n\delta_{al}}\delta_{al} + C_{n\delta_{er}}\delta_{er} + C_{n\delta_{el}}\delta_{el} + C_{n\delta_{fr}}\delta_{fr} + C_{n\delta_{fl}}\delta_{fl}$$

Equations (6) and (9) make obvious the aerodynamic forces and moments produced by each control surface. This is useful to model the fault effects and the redundancies provided by the healthy control surfaces.

The FDI/FTC problem is first an attitude control problem, thus the heading angle ψ, the x and y coordinates are not studied in the sequel.

With regard to the kinematic relations, the bank angle and the pitch angle time derivatives are (Boiffier, 1998):

$$\dot{\phi} = p + q\sin\phi\tan\theta + r\cos\phi\tan\theta$$

$$\dot{\theta} = q\cos\phi - r\sin\phi$$

$$\tag{10}$$

The relationship between the time derivative of the position of the aircraft's centre of gravity ξ, the transformation matrix $\mathbf{T_{bE}}$ and the linear velocities μ allows to write:

$$\dot{z} = -u \sin\theta + v \sin\phi \cos\theta + w \cos\phi \cos\theta \tag{11}$$

Let $\mathbf{X} = (\phi\ \theta\ V\ \alpha\ \beta\ p\ q\ r\ z)^T$ the state vector and $\mathbf{U} = (\delta_x\ \delta_{ar}\ \delta_{al}\ \delta_{fr}\ \delta_{fl}\ \delta_{er}\ \delta_{el})^T$ the control vector. All the state vector is measured and $\mathbf{Y}$ is the measure vector. From above, the model of the UAV can be written as a nonlinear model affine in the control

$$\dot{\mathbf{X}} = f(\mathbf{X}) + g(\mathbf{X})\mathbf{U} \tag{12}$$
$$\mathbf{Y} = \mathbf{CX}$$

Practically, the nonlinear aircraft model has been implemented with MATLAB in a *sfunction*. In the fault-free mode, for a given operating point $\{\mathbf{X_{e0}}, \mathbf{U_{e0}}\}$, where $\mathbf{U_{e0}}$ denotes the trim positions of the controls, the linearized model of the aircraft can be written as

$$\dot{\mathbf{x}} = \mathbf{Ax} + \mathbf{Bu} \tag{13}$$
$$\mathbf{y} = \mathbf{Cx} \tag{14}$$

2.1 Fault model

In the fault-free mode, the control surface deflections are constrained: asymmetrical aileron deflections produce the roll control, pitch is achieved through deflecting both ruddervators in the same direction and yaw is achieved through deflecting both ruddervators in opposite direction. As for the flaps, their deflection is symmetrical.

The faults considered are stuck control surfaces. For $t \geq t_f$, the faulty control vector $\mathbf{U^f}(t) = \mathcal{U}^\mathbf{f}$, where t_f is the fault-time and $\mathcal{U}^\mathbf{f}$ are the stuck control surface positions. For the simulations, a fault is modeled as a rate limiter response to a step. The slew rate is chosen equal to the maximum speed of the actuators. Let $\mathbf{U^h}$ be the remaining surfaces, then the state equation (12) in faulty mode becomes:

$$\dot{\mathbf{X}} = f(\mathbf{X}) + g^f(\mathbf{X})\mathbf{U^f} + g^h(\mathbf{X})\mathbf{U^h} \tag{15}$$

3. The nominal controller

A linear state feedback controller with reference tracking is designed. It is based on an EA method which allows to set the aircraft handling qualities (Magni et al., 1997). This method allows to set the modes of the closed-loop (CL) aircraft with respect to the standards (MIL-HDBK-1797, 1997) and to decouple some state and control variables from some modes. The design is based on the fault-free linearized model (13) which modal analysis shows that the spiral mode is open-loop (OL) unstable.

Let $\tilde{\mathbf{Y}} = (\phi\ \beta\ V\ z)$ the tracked vector and $\tilde{\mathbf{Y}}_{\mathbf{ref}}$ the reference vector. The autopilot is depicted in figure 2 and the nominal control law is:

$$\mathbf{u} = \mathbf{L}\zeta + \mathbf{Kx} \tag{16}$$

where $\dot{\zeta} = \tilde{\mathbf{Y}}_{\mathbf{ref}} - \tilde{\mathbf{Y}}$ augments the state vector with the state variables which have to be tracked to zero and

$$\dot{\zeta} = \left(\varepsilon_\phi\ \varepsilon_\beta\ \varepsilon_V\ \varepsilon_z\right)^T \tag{17}$$
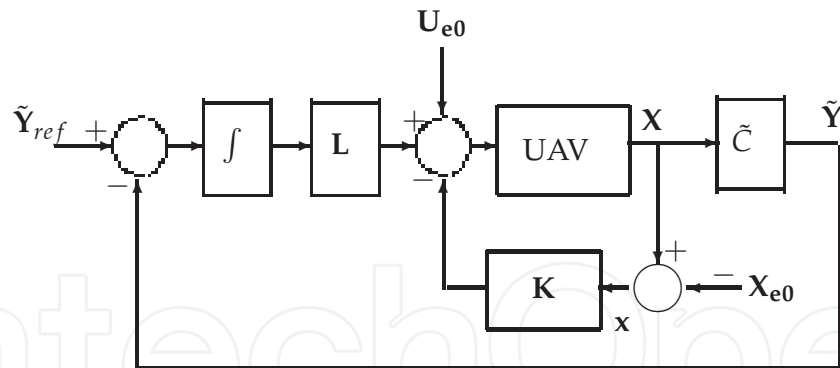
Fig. 2. The UAV control law

For a straight and level flight stage, Table 1 illustrates the EA strategy. A 0 means that the mode and the state variable or the control are decoupled. On the contrary, an × means that they are coupled.

In the fault-free mode, the ruddervators produce the pitch and the yaw, thus the longitudinal and the lateral axis are coupled. To take this into account, the autopilot is designed by considering the complete linearized model of the aircraft (13). For example, a coupling has been set between the spiral mode and the angle of attack which are a lateral mode and a longitudinal state variable respectively. This is illustrated by the highlighted cells in Table 1.

This approach significantly differs from the classical method which consists in designing two autopilots, one for the longitudinal axis, another one for the lateral axis. However, from the FTC point of view, a control surface failure upsets the equilibrium of forces and moments and produce significant couplings between longitudinal and lateral axis. Because of this, the method adopted to design the nominal autopilot could be used to design the fault-tolerant controllers. From (13), (16) and (17)

$$\begin{pmatrix} \dot{\mathbf{x}} \\ \dot{\zeta} \end{pmatrix} = \begin{pmatrix} \mathbf{A} + \mathbf{BK} & \mathbf{BL} \\ -\tilde{\mathbf{C}} & \mathbf{0} \end{pmatrix} \begin{pmatrix} \mathbf{x} \\ \zeta \end{pmatrix} + \begin{pmatrix} \mathbf{0} \\ \mathbf{I} \end{pmatrix} (\tilde{Y}_{ref}) \tag{18}$$

with $\tilde{\mathbf{C}} \in \mathbb{R}^{4 \times 9}$ and $\tilde{\mathbf{C}}(i,j) = 1$ for $\{i,j\} = \{1,1\}, \{2,5\}, \{3,3\}, \{4,9\}$ else $\tilde{\mathbf{C}}(i,j) = 0$.

Matrices $\mathbf{K} \in \mathbb{R}^{7 \times 9}$ and $\mathbf{L} \in \mathbb{R}^{7 \times 4}$ are computed in order to set the state space matrix's eigenvalues and eigenvectors in (18). These latter define the aircraft's modes. The state space matrix in (18) also writes:

$$\begin{pmatrix} \mathbf{A} & \mathbf{0} \\ -\tilde{\mathbf{C}} & \mathbf{0} \end{pmatrix} + \begin{pmatrix} \mathbf{B} \\ \mathbf{0} \end{pmatrix} (\mathbf{K} \ \mathbf{L}) = \mathbf{F} + \mathbf{G} (\mathbf{K} \ \mathbf{L}) \tag{19}$$

Let λ_i the ith eigenvalue (or closed-loop pole) corresponding to the eigenvector $\overrightarrow{\mathbf{v}}^i \in \mathbb{R}^{13}$, next

$$\left(\mathbf{F} + \mathbf{G} (\mathbf{K} \ \mathbf{L})\right) \overrightarrow{\mathbf{v}}^i = \lambda_i \overrightarrow{\mathbf{v}}^i \tag{20}$$

let

$$\overrightarrow{\mathbf{w}}^i = (\mathbf{K} \ \mathbf{L}) \overrightarrow{\mathbf{v}}^i \in \mathbb{R}^7 \tag{21}$$

then

$$\left(\mathbf{F} - \lambda_i \mathbf{I} \ \mathbf{G}\right) \begin{pmatrix} \overrightarrow{\mathbf{v}}^i \\ \overrightarrow{\mathbf{w}}^i \end{pmatrix} = \overrightarrow{\mathbf{0}} \tag{22}$$

mode	short period	phugoid	throttle	roll	dutchroll	spiral,ε_ϕ	ε_β	$\varepsilon_V,\varepsilon_z$
OL poles	$-4.2\pm9.6i$	$-0.03\pm0.5i$	-0.0002	-21	$-1.7\pm5.6i$	0.073		
CL poles	$-10\pm10i$	$-2\pm2i$	-1	-100	$-5\pm5i$	$-1\pm.25i$	-1.5	$-1\pm.5i$
eigenvector	$\vec{v}^{1,2}$	$\vec{v}^{3,4}$	$\vec{v}^{5}$	$\vec{v}^{6}$	$\vec{v}^{7,8}$	$\vec{v}^{9,10}$	$\vec{v}^{11}$	$\vec{v}^{12,13}$
ϕ	0	0	0	$\times$	$\times$	$\times$	$\times$	$\times$
θ	$\times$	$\times$	$\times$	0	0	$\times$	0	$\times$
V	$\times$	$\times$	$\times$	0	0	0	0	$\times$
α	$\times$	$\times$	$\times$	0	0	$\times$	0	$\times$
β	0	0	0	$\times$	$\times$	$\times$	$\times$	$\times$
p	0	0	0	$\times$	$\times$	$\times$	$\times$	0
q	$\times$	$\times$	$\times$	0	0	$\times$	0	$\times$
r	0	0	0	$\times$	$\times$	$\times$	$\times$	0
z	$\times$	$\times$	$\times$	$\times$	$\times$	0	$\times$	$\times$
ε_Φ	$\times$	$\times$	$\times$	$\times$	$\times$	$\times$	$\times$	$\times$
ε_β	$\times$	$\times$	$\times$	$\times$	$\times$	0	$\times$	$\times$
ε_V	$\times$	$\times$	$\times$	$\times$	$\times$	$\times$	$\times$	$\times$
ε_z	$\times$	$\times$	$\times$	$\times$	$\times$	$\times$	$\times$	$\times$
δ_x	$\times$	$\times$	$\times$	$\times$	$\times$	$\times$	$\times$	$\times$
δ_{ar}	0	0	0	$\times$	$\times$	$\times$	$\times$	0
δ_{al}	0	0	0	$\times$	$\times$	$\times$	$\times$	0
δ_{fr}	0	0	0	0	0	0	0	0
δ_{fl}	0	0	0	0	0	0	0	0
δ_{er}	$\times$	$\times$	$\times$	$\times$	$\times$	0	$\times$	$\times$
δ_{el}	$\times$	$\times$	$\times$	$\times$	$\times$	0	$\times$	$\times$

Table 1. Eigenstructure assignment strategy, airspeed $25ms^{-1}$, height $200m$

$(\mathbf{F}-\lambda_i\mathbf{I}\ \mathbf{G})$ is a 13×20 matrix and the size of its null space is equal to the number of control inputs, here seven. In order to set the eigenvector structure (Table 1) while reducing the solution space, some constraints are added. To hide the ith mode to the jth state variable or control input, a mask is introduced such that

$$\mathbf{mask}_i = \begin{pmatrix} \overset{1}{0} \cdots 0 \overset{j}{1} 0 \cdots \overset{20}{0} \end{pmatrix} \tag{23}$$

In order to find a unique solution vector, for each eigenvalue λ_i, six masks are defined and the system to solve writes

$$\begin{pmatrix} \mathbf{F}-\lambda_i\mathbf{I}\ \mathbf{G} \\ \mathbf{mask_{i1}} \\ \dots \\ \mathbf{mask_{i6}} \end{pmatrix} \begin{pmatrix} \overrightarrow{\mathbf{v}}^i \\ \overrightarrow{\mathbf{w}}^i \end{pmatrix} = \overrightarrow{\mathbf{0}} \tag{24}$$

Let $\mathbf{P}=\left(\overrightarrow{\mathbf{v}}^1\dots\overrightarrow{\mathbf{v}}^{13}\right)$ and $\mathbf{Q}=\left(\overrightarrow{\mathbf{w}}^1\dots\overrightarrow{\mathbf{w}}^7\right)$, then according to (21), matrices $\mathbf{K}$ and $\mathbf{L}$ write:

$$\left(\mathbf{K}\ \mathbf{L}\right)=\mathbf{Q}\mathbf{P}^{-1} \tag{25}$$

Fig. 4 shows the nominal autopilot functionning in the $[0s,16s]$ fault-free time interval.

4. Fault diagnosis

The class of faults addressed here are stuck control surfaces. However, the proposed diagnosis system can also deal with actuator the loss of efficiency.

To process for the faults, the diagnosis system could be realized by measuring the actuator positions. This approach which requires potentiometers, wiring and acquisition board is complex to implement and induces an increase of weight. Without these measurements, the control inputs appear as unknown inputs which have to be estimated. This can be achieved by the use of observers able to estimate the unknown inputs of a system.

In this connection, the problem of unknown, constant or slowy varying input estimation using banks of Kalman filters is discussed in (Kobayashi & Simon, 2003), (Ducard & Geering, 2008). The unknown inputs are declared as state variables, under the condition that the system is observable, the problem consists in estimating an augmented state vector.

However, to catch for the actuator fault transients, the observer has to estimate time varying inputs. Such an estimation is possible if these inputs are observable. The input observability problem was addressed by Patton in (Hou & Patton, 1998) who gave some necessary and sufficient conditions to prove input observability for linear time invariant systems with unknown initial conditions.

As far as the observer is concerned, Xiong (Xiong & Saif, 2003) proposed an Unknown Input Decoupled Functionnal Observer (UIDFO) which has no boundedness conditions as for time varying inputs and does not require differentiation of the measured outputs.

The fact remains that control surfaces offer redundancies that make aileron failures not isolable. In these conditions, an active diagnosis strategy has to be considered.

Input observability of the UAV is studied in subsection 4.1, the UIDFO is briefly described in subsection 4.2 and a diagnosis system based on a bank of UIDFO is detailed in subsection 4.3. The active diagnosis strategy is presented in subsection 4.4.

4.1 Input observability
Given, the linearized model (13).

Definition 1. *The input $u(t)$ is said to be observable if $y(t) = 0$ for $t \geq 0$ implies $u(t) = 0$ for $t > 0$* (Hou & Patton, 1998).

Let $\lambda \in \mathbb{C}$, $\Sigma_{\mathbf{sys}}$ and $\Sigma_{\mathbf{AC}}$ refer to the system matrix and the observability pencil respectively, they write:

$$\Sigma_{\mathbf{sys}} = \begin{pmatrix} \mathbf{A} & \mathbf{B} \\ \mathbf{C} & \mathbf{D} \end{pmatrix} - \lambda \begin{pmatrix} \mathbf{I} & \mathbf{0} \\ \mathbf{0} & \mathbf{0} \end{pmatrix} \text{ and } \Sigma_{\mathbf{AC}} = \begin{pmatrix} \mathbf{A} \\ \mathbf{C} \end{pmatrix} - \lambda \begin{pmatrix} \mathbf{I} \\ \mathbf{0} \end{pmatrix} \tag{26}$$

Kroenecker's theory of singular pencils shows that any pencil $\lambda \mathbf{M} - \mathbf{N}$ with dimension $m \times n$ can be brought into the canonical quasidiagonal form:

$$\mathbf{P}(\lambda \mathbf{M} - \mathbf{N})\mathbf{Q} = \begin{pmatrix} \lambda \mathbf{M_c} - \mathbf{N_c} & \times & \times & \times \\ & \lambda \mathbf{I} - \mathbf{N_f} & \times & \times \\ & & \lambda \mathbf{M_\infty} - \mathbf{I} & \times \\ & & & \lambda \mathbf{M_r} - \mathbf{N_r} \end{pmatrix} \tag{27}$$

- **P** and **Q** are nonsingular constant matrices with dimensions $m \times m$ and $n \times n$.

- the finite eigenvalues are in the square and regular pencil $\lambda \mathbf{I} - \mathbf{J_f}$ and $\mathbf{J_f}$ is in Jordan canonical form. It is built with Jordan blocks $\mathbf{J_{f_i}}$ with dimension $i \times i$.

- the infinite eigenvalues are in the square and regular pencil $\lambda \mathbf{J_\infty} - \mathbf{I}$ and $\mathbf{J_\infty}$ is compound with Jordan blocks $\mathbf{J_{\infty_i}}$ of size $i \times i$.

- $\lambda \mathbf{M_r} - \mathbf{N_r}$ is a singular pencil and has a block diagonal structure, each block takes the form $\lambda \mathbf{M_{r_i}} - \mathbf{N_{r_i}} = \lambda \begin{pmatrix} \mathbf{I} \\ \mathbf{0}^T \end{pmatrix} - \begin{pmatrix} \mathbf{0}^T \\ \mathbf{I} \end{pmatrix}$ with dimension $r_{i+1} \times r_i$. **0** stands for zero vector and $\mathbf{0}^T$ denotes its transpose. The r_i are called Kroenecker's row indices.

- $\lambda \mathbf{M_c} - \mathbf{N_c}$ is a singular pencil and has a block diagonal structure, each block takes the form : $\lambda \mathbf{M_{c_j}} - \mathbf{N_{c_j}} = \lambda \begin{pmatrix} \mathbf{I} & \mathbf{0} \end{pmatrix} - \begin{pmatrix} \mathbf{0} & \mathbf{I} \end{pmatrix}$. The $c_j \times c_{j+1}$ are called Kroenecker's column indices.

This decomposition is applied to $\mathbf{\Sigma_{sys}}$ and $\mathbf{\Sigma_{AC}}$. The following theorem contains a numerically effective test for input observability:

Theorem 1. *System (13) is input observable if and only if the block* $\lambda \mathbf{M_{c_{sys}}} - \mathbf{N_{c_{sys}}}$ *vanishes in equation (27) and* $dim(\mathbf{J_{f_{sys}}}) = dim(\mathbf{J_{f_{AC}}})$ *(Hou et Patton)(Hou & Patton, 1998).*

Nevertheless, due to the numerical unreliability of the computation, this form is not suitable and the staircase form, computed with the GUPTRI algorithm, is used to exhibit the Kroenecker form (Demmel & Kågstrom, 1993).
All the state vector is measured and theorem 1 is applied to assess the ruddervator observability. For this outpout vector, the matrix system and the observability pencil have the following structures:

- $\mathbf{\Sigma_{AC}}$ has no finite eigenvalue, nine singular pencils with Kronecker raw indice equal to one,

- $\mathbf{\Sigma_{sys}}$ has no finite eigenvalue, seven singular pencils with Kronecker raw indice equal to one and two 2×2 jordan blocks containing infinite eigenvalues.

According to theorem 1 the ruddervator positions are observable. With the same measured outputs, theorem 1 is applied to assess the aileron observability. The matrix system and the observability pencil have the following structure:

- $\mathbf{\Sigma_{AC}}$ is unchanged

- $\mathbf{\Sigma_{sys}}$ has no finite eigenvalue, one singular pencil with Kronecker column indice equal to one, eight singular pencils with Kronecker raw indice equal to one and one 2×2 jordan block containing infinite eigenvalues.

Due to the presence of the singular pencil with Kronecker column equal to one, the aileron positions are not both observable. Thus, if one of the ailerons breaks down, the faulty control is not isolable. This is depicted in Fig. 3 where a down lock position of the left aileron has the same effects as a top lock position of the right aileron. In this case, an active diagnosis must be used to discriminate the faulty control surface.
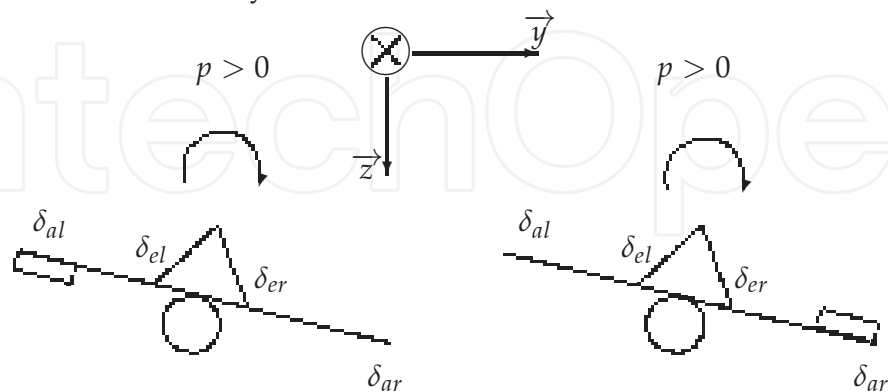
Fig. 3. Aerodynamic effects induced by right and left aileron failures

4.2 The unknown input decoupled functional observer

In this part, results established in (Xiong & Saif, 2003) are recalled. The following dynamic system driven by both known and unknown inputs is considered

$$\dot{\mathbf{x}} = \mathbf{Ax} + \mathbf{Bu} + \mathbf{Gd} \qquad (28)$$
$$\mathbf{y} = \mathbf{Cx}$$

where $\mathbf{x} \in \mathbb{R}^n$ is the state vector, $\mathbf{u} \in \mathbb{R}^m$ is the known input vector, $\mathbf{d} \in \mathbb{R}^\ell$ is the unknown input vector and $\mathbf{y} \in \mathbb{R}^o$ is the output vector. $\mathbf{A}$, $\mathbf{B}$, $\mathbf{G}$ and $\mathbf{C}$ are matrices with appropriate dimensions, $\mathbf{C}$ and $\mathbf{G}$ are assumed to be full rank.

The UIDFO detailed in (Xiong & Saif, 2003) provides an estimation $\hat{\mathbf{d}}$ of the unknown input $\mathbf{d}$ and an estimation $\mathbf{z}$ of linear combination of state $\mathbf{Tx}$. Theoretically, no boundedness conditions are required for the unknown inputs and their derivatives.

$$\dot{\mathbf{z}} = \mathbf{Fz} + \mathbf{Hy} + \mathbf{TBu} + \mathbf{TG}\hat{\mathbf{d}} \qquad (29)$$
$$\hat{\mathbf{d}} = \gamma(\mathbf{Wy} - \mathbf{Ez}) \text{ with } \gamma \in \mathbb{R}^{*+}$$

Matrices $\mathbf{F}, \mathbf{H}, \mathbf{T}, \mathbf{W}$ and $\mathbf{E}$ are all design parameters. in order to satisfy the following conditions

$$\begin{cases} \mathbf{FT} - \mathbf{TA} + \mathbf{HC} = 0 & \mathbf{F} \text{ is stable,} \\ \mathbf{E} = (\mathbf{TG})^T \mathbf{P} & \text{with } \mathbf{P} \text{ solution of: } \mathbf{PF} + \mathbf{F}^T \mathbf{P} = -\mathbf{Q} \\ & \text{and } \mathbf{Q}, \text{ a semi-positive definite matrix,} \\ \mathbf{ET} = \mathbf{G}^T \mathbf{T}^T \mathbf{PT} = \mathbf{WC} \\ rank(\mathbf{TG}) = rank(\mathbf{G}) = \ell \end{cases} \qquad (30)$$

These matrices exist if and only if

(i) $rank(\mathbf{CG}) = rank(\mathbf{G})$,

(ii) all unstable transmission zeros of system $(\mathbf{A}, \mathbf{G}, \mathbf{C})$ are unobservable modes of $(\mathbf{A}, \mathbf{C})$.

To prove their existence and to calculate them, system (28) is transformed into "*Special Coordinate Basis*" (SCB) (X.Liu et al., 2005).

4.3 Diagnosis system performed with a bank of UIDFO

The right aileron, the left aileron, the right ruddervator and the left ruddervator positions are unknown. In order to estimate each one of these unknown input positions, a bank of four UIDFOs is implemented. However, it has been proven above that the ailerons are not both input observable. It means that, if one of these two controls is faulty, one of the two estimations is wrong whereas the other is right, but in any case it is impossible to know which one is which.

Let $\hat{\delta}_{ar}$, $\hat{\delta}_{al}$, $\hat{\delta}_{er}$ and $\hat{\delta}_{el}$ the positions estimated by each UIDFO, δ_{ar}, δ_{al}, δ_{er} and δ_{el} the known control inputs computed by the nominal controller and $\bar{\delta}_{ar}$, $\bar{\delta}_{al}$, $\bar{\delta}_{er}$ and $\bar{\delta}_{el}$ the unknown actual control surface positions. In the fault-free mode, the actual control surface positions are equal to those computed by the controller and to their estimations. When an actuator breaks down, the faulty actual control surface position is equal to its estimation but differs from that computed by the controller. Residuals are obtained by processing the differences between the positions computed by the controller with the estimated positions. The fault detection and isolation process consists in monitoring residuals by comparing them with thresholds.

The first UIDFO estimates the unknown right aileron actual position $\bar{\delta}_{ar}$ by processing the measurement vector $\mathbf{y}$ and the known input $\mathbf{u_1} = (\delta_{al}, \delta_{er}, \delta_{el})^T$. Let b_{δ_i} the column of the control matrix B associated with the δ_i control input, then $\mathbf{B_1} = (b_{\delta_{al}}, b_{\delta_{er}}, b_{\delta_{el}})^T$ and $\mathbf{G_1} = (b_{\delta_{ar}})$,

$$\dot{\mathbf{z}}_1 = \mathbf{F_1 z_1} + \mathbf{H_1 y} + \mathbf{T_1 B_1}(\delta_{al}, \delta_{er}, \delta_{el})^T + \mathbf{T_1 G_1}\hat{\delta}_{ar} \tag{31}$$
$$\hat{\delta}_{ar} = \gamma_1(\mathbf{W_1 y} - \mathbf{E_1 z_1})$$

The other three ones UIDFO equations write

$$\dot{\mathbf{z}}_2 = \mathbf{F_2 z_2} + \mathbf{H_2 y} + \mathbf{T_2 B_2}(\delta_{ar}, \delta_{er}, \delta_{el})^T + \mathbf{T_2 G_2}\hat{\delta}_{al} \tag{32}$$
$$\hat{\delta}_{al} = \gamma_2(\mathbf{W_2 y} - \mathbf{E_2 z_2})$$

with $\mathbf{B_2} = (b_{\delta_{ar}}, b_{\delta_{er}}, b_{\delta_{el}})^T$ and $\mathbf{G_2} = (b_{\delta_{al}})$,

$$\dot{\mathbf{z}}_3 = \mathbf{F_3 z_3} + \mathbf{H_3 y} + \mathbf{T_3 B_3}(\delta_{ar}, \delta_{al}, \delta_{el})^T + \mathbf{T_3 G_3}\hat{\delta}_{er} \tag{33}$$
$$\hat{\delta}_{er} = \gamma_3(\mathbf{W_3 y} - \mathbf{E_3 z_3})$$

with $\mathbf{B_3} = (b_{\delta_{ar}}, b_{\delta_{al}}, b_{\delta_{el}})^T$ and $\mathbf{G_3} = (b_{\delta_{er}})$,

$$\dot{\mathbf{z}}_4 = \mathbf{F_4 z_4} + \mathbf{H_4 y} + \mathbf{T_4 B_4}(\delta_{ar}, \delta_{al}, \delta_{er})^T + \mathbf{T_4 G_4}\hat{\delta}_{el} \tag{34}$$
$$\hat{\delta}_{el} = \gamma_4(\mathbf{W_4 y} - \mathbf{E_4 z_4})$$

with $\mathbf{B_4} = (b_{\delta_{ar}}, b_{\delta_{al}}, b_{\delta_{er}})^T$ and $\mathbf{G_4} = (b_{\delta_{el}})$.
For all the UIDFOs, condition (i) is assessed and condition (ii) is checked by computing the staircase forms of the system matrices $(\mathbf{A}, \mathbf{G_j}, \mathbf{C}, \mathbf{0})$ with $j = \{1, \ldots, 4\}$ and the observability pencil $(\mathbf{A}, \mathbf{C})$ with the GUPTRI algorithm.

Error signals are generated by comparison between the control positions δ_i and the estimated positions $\hat{\delta}_i$ where $\delta_i \in \{\delta_{ar}, \delta_{al}, \delta_{er}, \delta_{el}\}$. In order to avoid false alarm that may arise from the transient behavior, these signals are integrated on a duration τ to produce residuals r_{δ_i} such that

$$r_{\delta_i} = \left| \int_t^{t+\tau} \hat{\delta}_i(\theta) - \delta_i(\theta)d\theta \right| \tag{35}$$

Let σ_{δ_i} the corresponding threshold and μ_{δ_i} a logical state such that $\mu_{\delta_i} = 1$ if $r_{\delta_i} > \sigma_{\delta_i}$ else $\mu_{\delta_i} = 0$. Then, to detect and to partially isolate the faulty control surface, an incidence matrix is defined as follows:

Faulty control	$\mu_{\delta_{ar}}$	$\mu_{\delta_{el}}$	$\mu_{\delta_{al}}$	$\mu_{\delta_{er}}$
right aileron	1	0	1	0
left aileron	1	0	1	0
right ruddervator	0	0	0	1
left ruddervator	0	1	0	0

Table 2. The incidence matrix

This matrix reveals that fault on right aileron and fault on left aileron are not isolable.
In order to illustrate the above-mentioned concepts, three failure scenarios are studied: a non critical ruddervator loss of efficiency 50%, a catastrophic ruddervator locking and a non critical aileron locking. For the three cases, the fault occurs at faulty time $t_f = 16s$ whereas the UAV is turning and changing its airspeed (see Fig.4, Fig.7, Fig.10). These two manoeuvres involve both ailerons and ruddervators.

4.3.1 Ruddervator loss of efficiency

For the right ruddervator, a 50% loss of efficiency is simulated. The nominal controller is robust enough to accommodate for the fault as it is depicted in Fig.4. The actual control surface positions and their estimations are shown in Fig. 5. As far as the right ruddervator is concerned, after time t_f, its control signal differs from its estimated position and this difference renders the fault obvious. The residuals are depicted in Fig. 6, with respect to (35) and to the incidence matrix Tab. 2, the right ruddervator is declared to be faulty.

4.3.2 Ruddervator locking

At time t_f, the right ruddervator is stuck at position $0°$. As it is illustrated in Fig.7, the nominal controller cannot accommodate for the fault and the UAV is lost. The actual control surface positions and their estimations are shown in Fig.8, As regards the right ruddervator, its control signal differs from its estimated position and the residual analysis Fig.9 allows to declare this control surface to be faulty. However, the control and measurement vectors diverge quickly, thus the signal acquisition of the estimated positions has to be sampled fast.

4.3.3 Aileron locking

In the event of an aileron failure, the nominal controller is robust enough to accommodate for the fault. However, the incidence matrix shows that faults on right and left ailerons cannot be isolated. This is due to the redundancies offered by these control surfaces that are not input observable. This aspect is depicted in Fig. 10, 11, 12 where the left aileron locks at position $+5°$ at time $t_f = 16s$. Fig.10 shows that this fault is non critical (it is naturally accommodated by the right aileron). However, as it is shown in Fig. 11, both estimations of aileron positions are consistent and the corresponding residuals exceed the thresholds. As a consequence, it is not possible to isolate the faulty aileron.

4.4 Active diagnosis

To overcome this problem, an active fault diagnosis strategy is proposed. It consists in exciting one of the aileron (here the right aileron) with a small-amplitude sinusoidal signal. If the left aileron is stuck, the measures contain a sinusoidal component which is detected with a selective filter. If the right aileron is stuck, the sinusoidal excitation cannot affect the state vector and the measures do not contain the sinusoidal components. This point is depicted in Fig. 13, a fault is simulated on the left aileron next to the right aileron. In the first case, the left aileron is stuck at $-5°$, after the fault has been detected, the right aileron is excited with a $1° sin(20t)$ signal. This component distinctly appears in the estimation of the left aileron position and allows to declare the left aileron faulty. In the second case, the right aileron is stuck at $+5°$, after the fault has been detected, the right aileron is excited with the same sinusoidal signal. As this control surface is stuck, the sinusoidal signal does not appear in the estimation of the right aileron position and this control surface is declared faulty. Note that this method allows only to detect stuck ailerons. To deal with a loss of efficiency, three control surfaces are excited: the right aileron, the right and the left flaps. The excitation signals are such that they little affect the state and the measurement vectors. This is achieved by choosing the amplitudes of these excitations in the nullspace of the $(b_{\delta_{ar}}, b_{\delta_{fr}}, b_{\delta_{fl}})$ matrix or if the nullspace does not exist, the excitation vector can be chosen as the right singular vector corresponding with the smallest singular value of the $(b_{\delta_{ar}}, b_{\delta_{fr}}, b_{\delta_{fl}})$ matrix. If the right aileron is faulty, the excitation is not fulfilled and the measures contain a sinusoidal component. On the contrary, if the left aileron is faulty, the right aileron and the flaps fulfill the exctitation
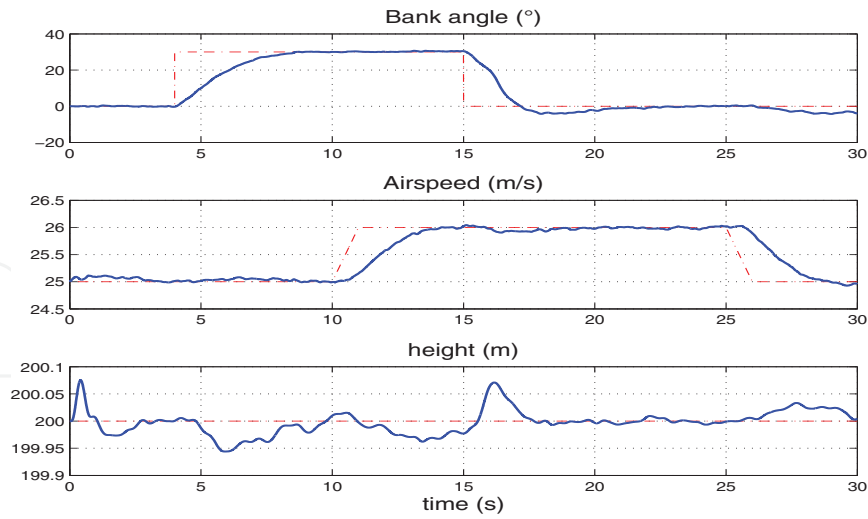
Fig. 4. Right ruddervator loss of efficiency: the tracked state variables
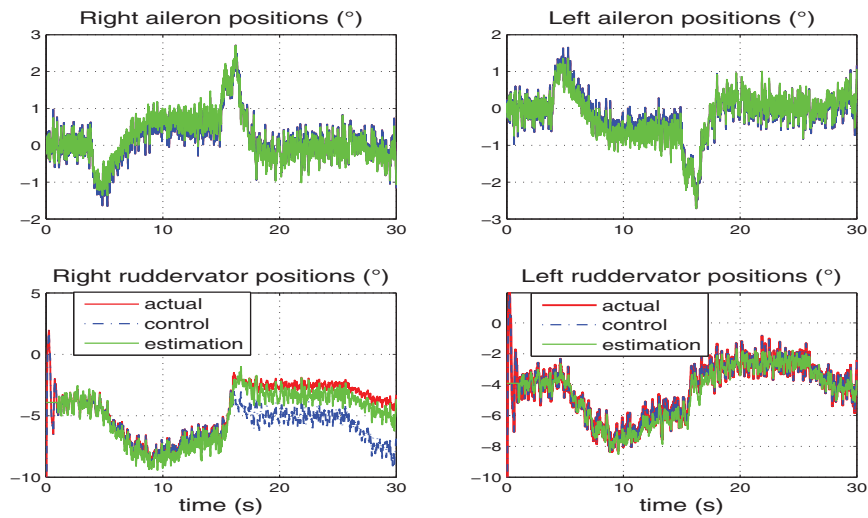

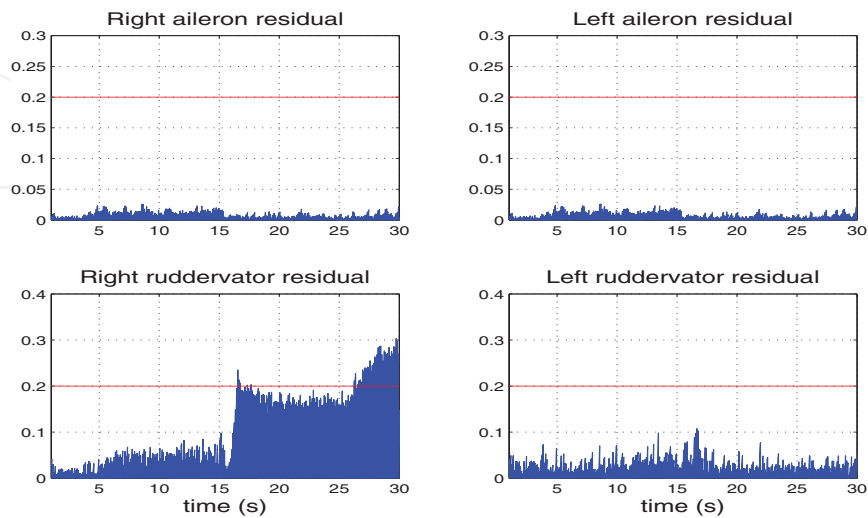Fig. 5. Right ruddervator failure: the estimation process

Fig. 6. Right ruddervator failure: the fault detection and isolation process
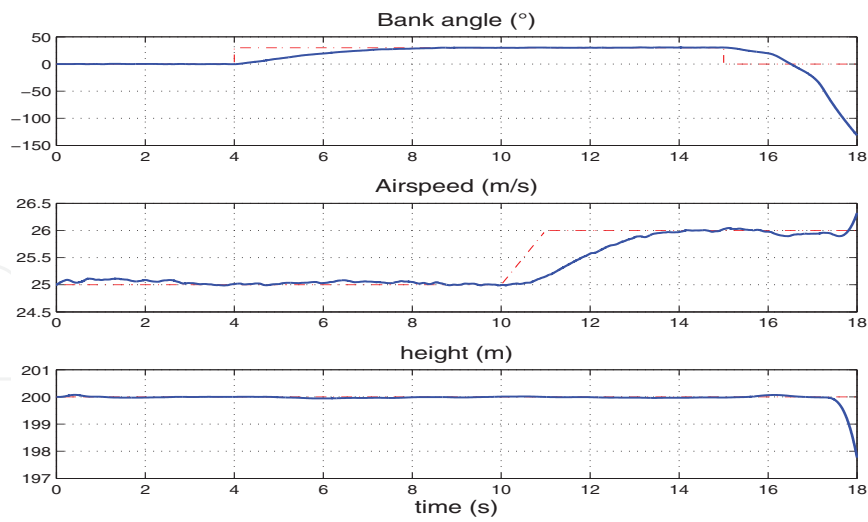
Fig. 7. Right ruddervator stuck: the tracked state variables
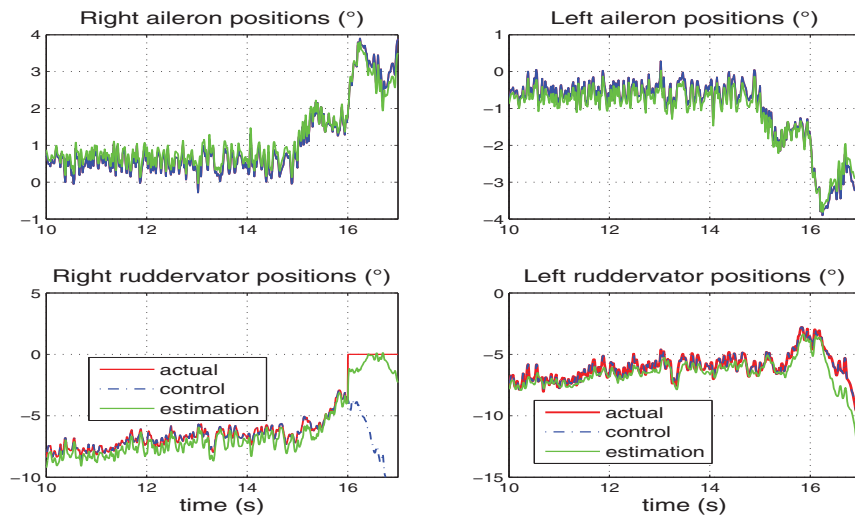

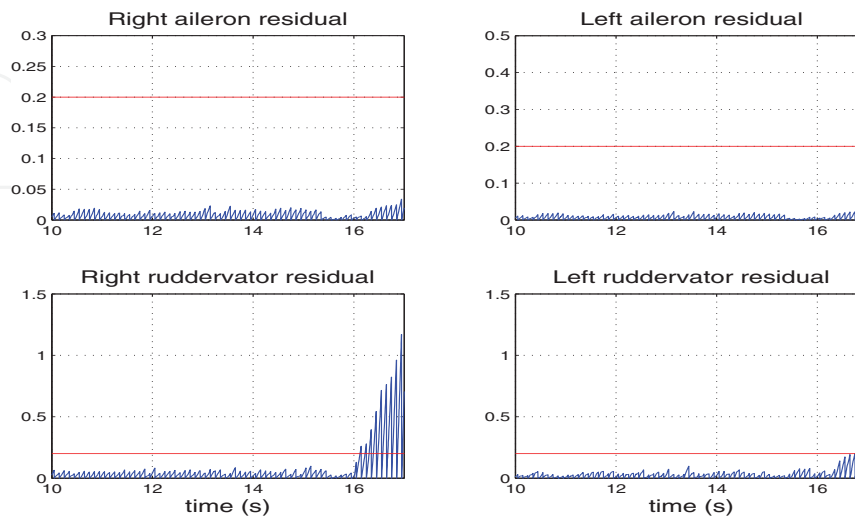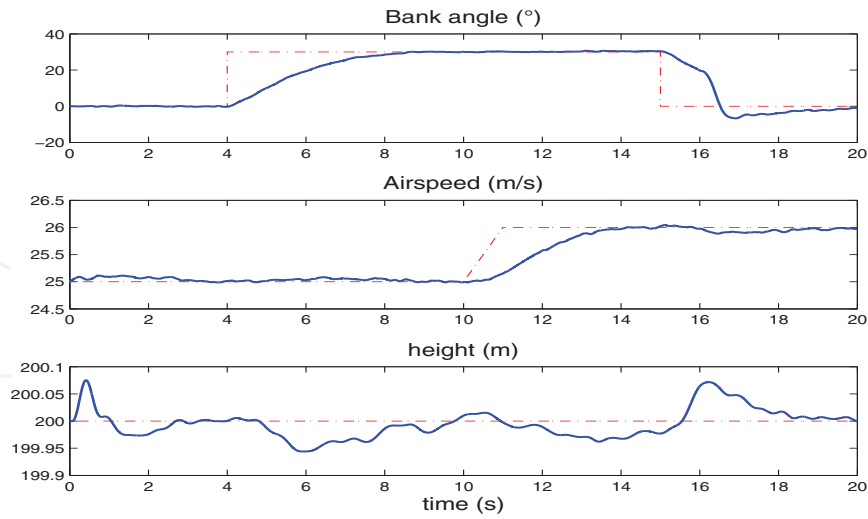
Fig. 8. Right ruddervator failure: the estimation process

Fig. 9. Right ruddervator failure: the fault detection and isolation process
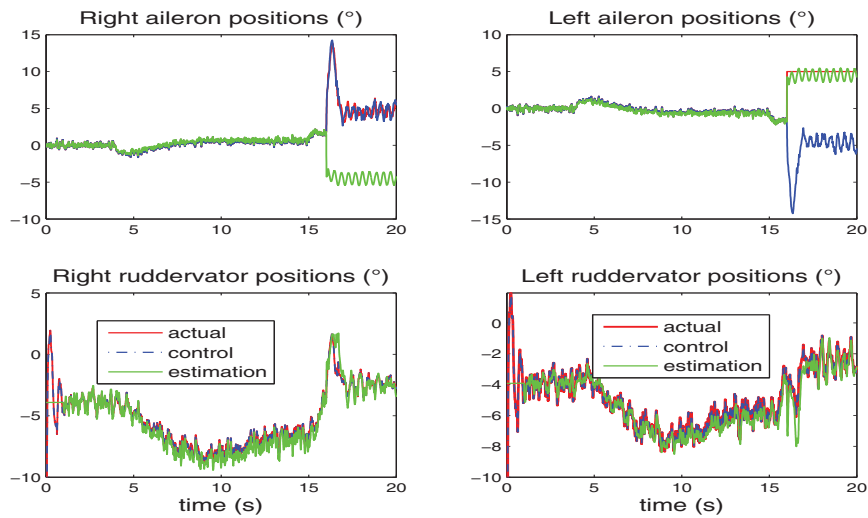
Fig. 10. Left aileron stuck: the tracked state variables

Fig. 11. Left aileron failure: the estimation process
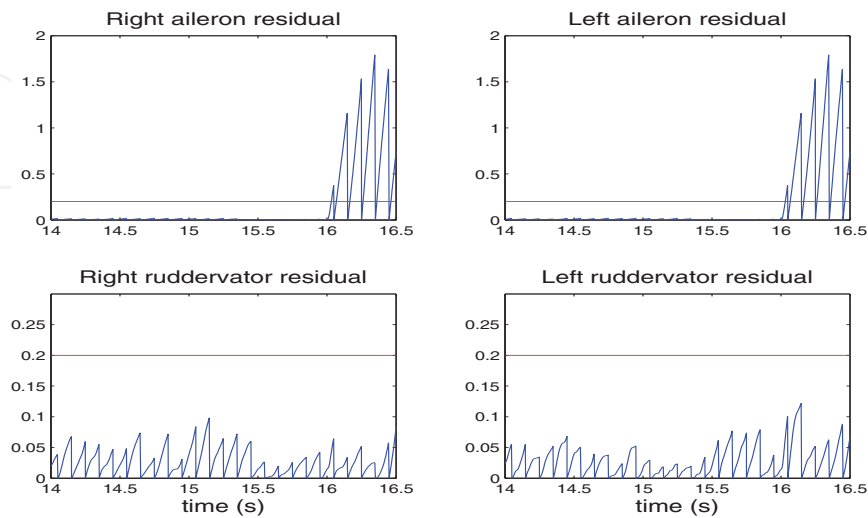
Fig. 12. Left aileron failure: the fault detection and isolation process
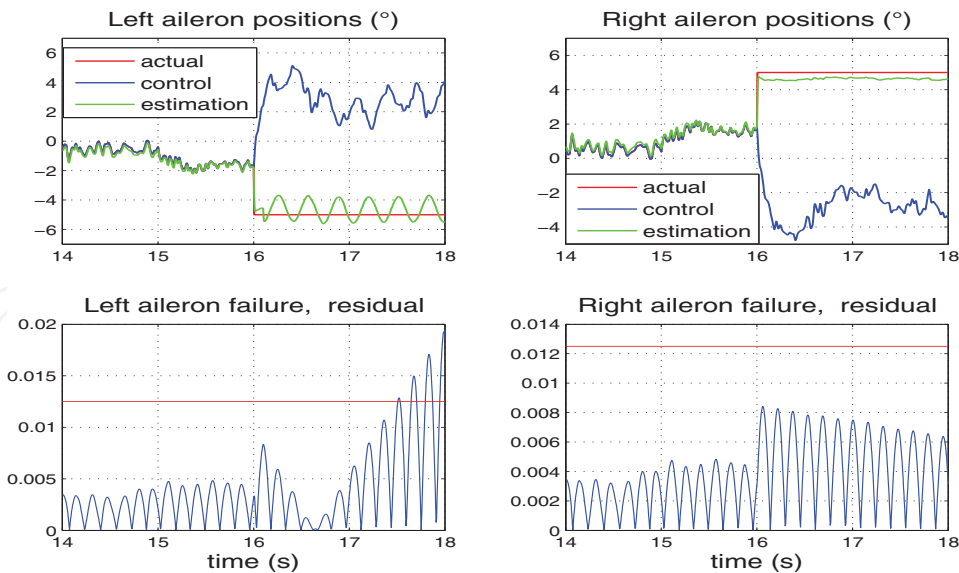
Fig. 13. Left or right aileron stuck: the active diagnosis method

signals, as these latter have no effect on the state vector, the measures do not contain sinusoidal components.

5. Fault-tolerant control

The faults considered are asymmetric stuck control surfaces. When one or several control surfaces are stuck, the balance of forces and moments is broken, the UAV moves away from the fault-free mode operating point and there is a risk of losing the aircraft. This risk is all the more so critical that it affects the ruddervators, these latter producing the pitch and the yaw moments.

So a fault may be accommodated only if an operating point exists and the design of the FTC follows this scheme.

1. It is assumed that the faulty control surface and the fault magnitude are known. This information is provided by the fault diagnosis system described above.

2. The deflection constraints of the remaining control surfaces are released *e.g* symmetrical deflections for flaps, asymmetrical deflections for ailerons.

3. For the considered faulty actuator and its fault position, a new operating point is computed.

4. For this new operating point a linear state feedback controller is designed with an EA strategy. This controller aims to maintain the aircraft handling qualities at their fault-free values.

5. The accommodation is achieved by implementing simultaneously the new operating point and the fault-tolerant controller.

5.1 Operating point computation

The operating point exists if the healthy controls offer sufficient redundancies and its value depends on:

- the considered flight stage,

- the faulty control surface,
- the fault magnitude.

In the following $\{\mathbf{X_e}, \mathbf{U_e}\}$ denote the operating point in faulty mode, $\mathbf{U_e^h}$ the trim positions of the remaining controls and $\mathbf{U^f}$ the faulty controls. According to (15) and when k control surfaces are stuck, computing an operating point is equivalent to solve the algebraic equation:

$$0 = f(\mathbf{X_e}) + g^h(\mathbf{X_e})\mathbf{U_e^h} + g^f(\mathbf{X_e})\mathbf{U^f} \tag{36}$$

To take into account the flight stage envelope and the remaining control surface deflections, the operating point computation is achieved with an optimization algorithm. This latter aims at minimizing the cost function:

$$J = q_V(V - V_{e_0})^2 + q_\alpha(\alpha - \alpha_{e_0})^2 + q_\beta(\beta - \beta_{e_0})^2 \tag{37}$$

under the following equality and inequality constraints:

- a control surface is stuck

$$\mathbf{U^f} = \mathcal{U}^f \tag{38}$$

- the flight envelope and the healthy control deflections are bounded:

$$\begin{cases} \mathbf{X_{min}} \leq \mathbf{X} \leq \mathbf{X_{max}} \\ \mathbf{U_{min}^h} \leq \mathbf{U^h} \leq \mathbf{U_{max}^h} \end{cases} \tag{39}$$

- according to the desired flight stage, some equality constraints are added
  - flight level

$$\begin{cases} \dot{\phi} = \dot{\theta} = \dot{V} = \dot{\alpha} = \dot{\beta} = \dot{p} = \dot{r} = \dot{q} = \dot{z} = 0 \\ \phi = p = q = r = 0 \end{cases} \tag{40}$$

  - climb or descent with a flight path equal to γ

$$\begin{cases} \dot{\phi} = \dot{\theta} = \dot{V} = \dot{\alpha} = \dot{\beta} = \dot{p} \quad = \dot{r} = \dot{q} = 0 \\ \phi = p = q = r = 0 \,, \quad \theta - \alpha = \gamma \end{cases} \tag{41}$$

  - turn

$$\begin{cases} \dot{\phi} = \dot{\theta} = \dot{V} = \dot{\alpha} = \dot{\beta} = \dot{p} = \dot{r} = \dot{q} = \dot{z} = 0 \\ p = q = 0 \,, \quad \phi = \phi_e \,, \quad r = r_e \end{cases} \tag{42}$$

This strategy aims at keeping the operating point in faulty mode the closest to its fault-free value. As the linearized model *i.e.* the state space and the control matrices strongly depends of the operating point, the open-loop poles (and consequently the open-loop handling qualities) are little modified.

The computation of an operating point for a faulty ruddervator is described in the sequel. The right ruddervator is stuck on its whole deflection range $[-20°, +20°]$ and the remaining controls are trimmed in order to maintain the UAV flight level with an airspeed close to $25m/s$ and an height equal to $200m$. The results of the computation are illustrated in Fig 14. They show that an operating point exists in the $[-13°, +3°]$ interval. However, for some fault positions, the actuator positions are close to their saturation positions. This will drastically limit the aircraft performance. For example, a fault in the $1°$ position can be compensated with a throttle trimmed at 90%. It is obvious that this value will limit the turning performance.

Indeed, during the turn, due to the bank angle, the lift force decreases and to keep a constant height, increasing the throttle control is necessary. As the throttle range is limited, the bank angle variations will be reduced. This is all the more critical that the aircraft has a lateral unstable mode. Note that, from now on, there are couplings between the longitudinal and the lateral axes. Indeed, to obtain these faulty operating points, the longitudinal and the lateral state variables are coupled *e.g.* the sideslip angle must differ from zero to achieve a flight level stage.

For each fault position in the $[-13°, +3°]$ interval, the operating point and the related linearized model are computed. The root locus is depicted in Fig. 15 and shows that the open-loop poles are little scattered.

To complete this work, similar studies should be conducted for the left ruddervator, the right and left ailerons.
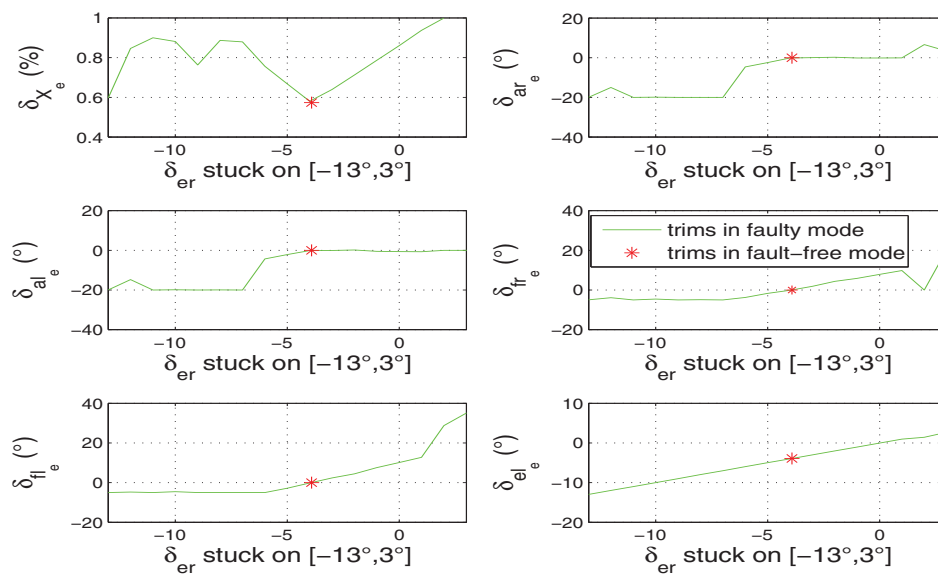
Fig. 14. Right ruddervator stuck, the remaining control trim positions
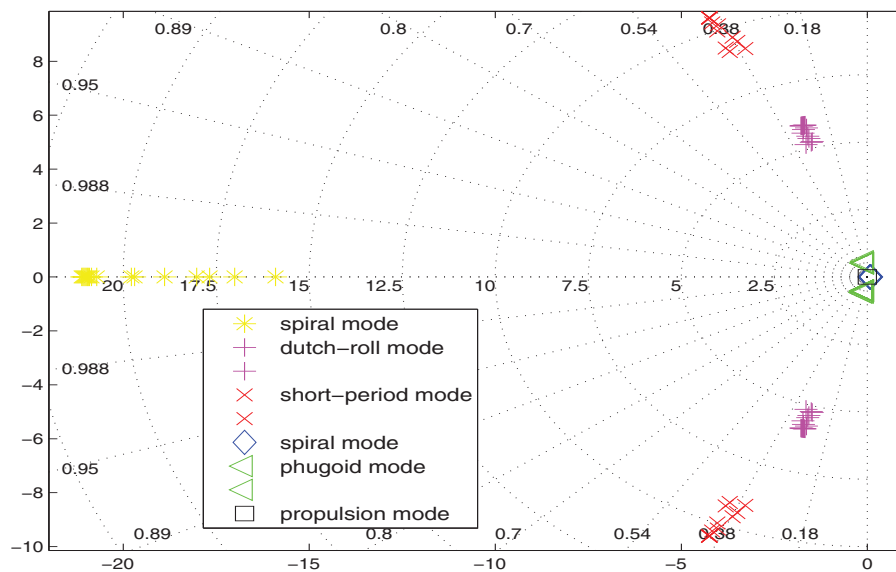
Fig. 15. Right ruddervator stuck, the poles's map

5.2 Fault-tolerant controller design

Fault-tolerant control (FTC) strategy has received considerable attention from the control research community and aeronautical engineering in the last two decades (Steinberg, 2005). An exhaustive and recent bibliographical review for FTC is presented in (Zhang & Jiang, 2008). Even though different methods use different design strategies, the design goal for reconfigurable control is in fact the same. That is, the design objective of reconfigurable control is to design a new controller such that post-fault closed-loop system has, in certain sense the same or similar closed-loop performance to that of the pre-fault system (Zhang & Jiang, 2006). In this work, the FTC objective consists in keeping the faulty UAV handling qualities identical to those existing in fault-free mode. Moreover, the tracked outputs (ϕ, β, V, z) should have the same dynamics that in fault-free mode. As the computation of the faulty operating point induced couplings between the longitudinal and the lateral axes, and as each healthy actuator is driven separately, FTC controllers identical to the nominal controller are kept, *i.e.* linear state feedback fault-tolerant controllers which design is based on an EA strategy. This is illustrated in Tab. 3 where the proposed EA strategy aims at accommodating a right ruddervator failure. Note that with respect to Tab. 1, the closed-loop poles are unchanged, but the eigenvectors are modified, particularly to decouple the modes from the faulty control. The design of the

mode	short period	phugoid	throttle	roll	dutchroll	spiral,ε_ϕ	ε_β	$\varepsilon_V,\varepsilon_z$
CL poles	$-10\pm10i$	$-2\pm2i$	-1	-100	$-5\pm5i$	$-1\pm.25i$	-1.5	$-1\pm.5i$
eigenvector	$\vec{v}^{1,2}$	$\vec{v}^{3,4}$	$\vec{v}^5$	$\vec{v}^6$	$\vec{v}^{7,8}$	$\vec{v}^{9,10}$	$\vec{v}^{11}$	$\vec{v}^{12,13}$
ϕ	×	0	×	×	×	×	×	×
θ	×	×	×	0	×	×	0	×
V	×	×	×	0	0	0	0	×
α	×	×	×	0	×	×	×	×
β	0	0	0	×	×	×	×	×
p	0	0	0	×	×	×	×	0
q	×	×	×	0	×	×	0	×
r	0	0	0	×	×	×	×	0
z	×	×	×	×	0	0	×	×
ε_Φ	×	×	×	×	×	×	×	×
ε_β	×	×	×	×	×	×	×	×
ε_V	×	×	×	×	×	×	×	×
ε_z	×	×	×	×	×	×	×	×
δ_x	0	×	×	×	×	×	×	×
δ_{ar}	×	0	0	×	×	×	×	0
δ_{al}	×	0	0	×	×	×	×	0
δ_{fr}	0	×	×	0	0	0	0	×
δ_{fl}	×	×	×	0	0	0	0	0
δ_{er}	0	0	0	0	0	0	0	0
δ_{el}	×	×	0	×	×	×	×	×

Table 3. Fault-tolerant controller, EA strategy for a ruddervator failure

FTC is similar to those presented in section 3. Similar studies could be conducted for the other control surfaces.

5.3 Fault-tolerant controller implementation

A fault is described by the type of control surface and its fault magnitude. This information is provided by the FDI system studied above. For a given fault, a new operating point and a FTC controller must be theoretically computed. As far as the operating points are concerned, they

are precomputed, tabulated and selected with respect to the fault. In the same way, a FTC should be designed for each operating point and its corresponding linearized model. This method has been adopted to compensate for right ruddervator failures. Practically, it enables to accommodate for them in the $[-5°, 0°]$ interval with a $1°$ step study. Consequently, six fault-tolerant controllers should be designed.

In order to reduce this number and for the six faulty linearized models, a single fault-tolerant controller is kept, the one which minimizes the scattering of the poles. For a right ruddervator failure, this fault-tolerant controller is the one designed for a $-2°$ fault position.

Outside this interval, the faults are too severe to be accommodated.

5.4 Results of simulations

Results of simulations are depicted in Fig. 16. The right ruddervator is stuck in the $0°$ position at time $t_f = 16s$. This case is similar to the one studied in the paragraph 4.3.2. After time t_f, the fault is detected, isolated and its magnitude is estimated, then the fault-tolerant controller efficiently compensates for the fault and the aircraft can continue to fly and to maneuver. However, for the reasons explained in subsection 5.1, the bank angle cannot exceed $10°$ and the nonlinear effects due to the throttle saturation (see. Fig. 16) affects the dynamics of the airspeed.

The same fault-tolerant controller is tested for various stuck positions simulated in the $[-5°, 0°]$ interval and occuring at time $t_f = 16s$. As it is shown in Fig. 18, all these faults are accommodated with this unique fault-tolerant controller.
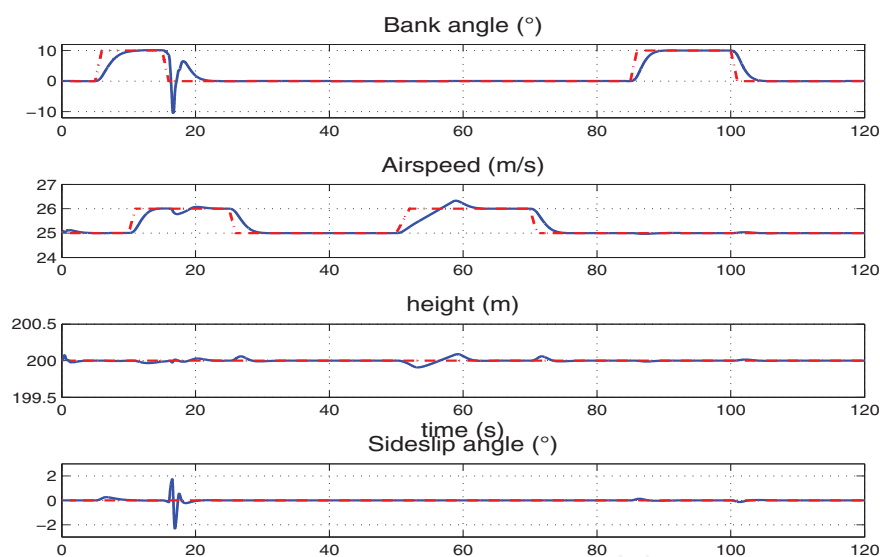

Fig. 16. Right ruddervator stuck, the tracked state variables

6. Conclusion

A UAV model has been designed to deal with asymmetrical control surfaces failures that upset the equilibrium of moments and produce couplings between the longitudinal and the lateral axes. The nominal controller aims at setting the UAV handling qualities and it is based on an eigenstructure assignment strategy. Control surface positions are not measured and, in order to diagnose faults on these actuators, input observability has been studied. It has proven that faults on the ailerons are not isolable. Next, a bank of Unknown Input Decoupled Functional
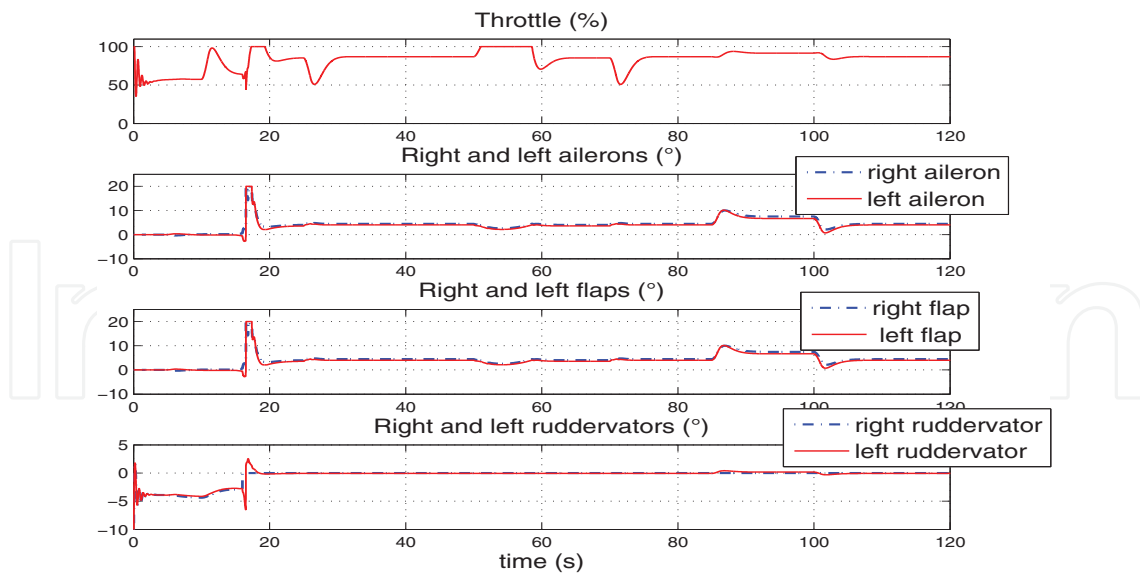
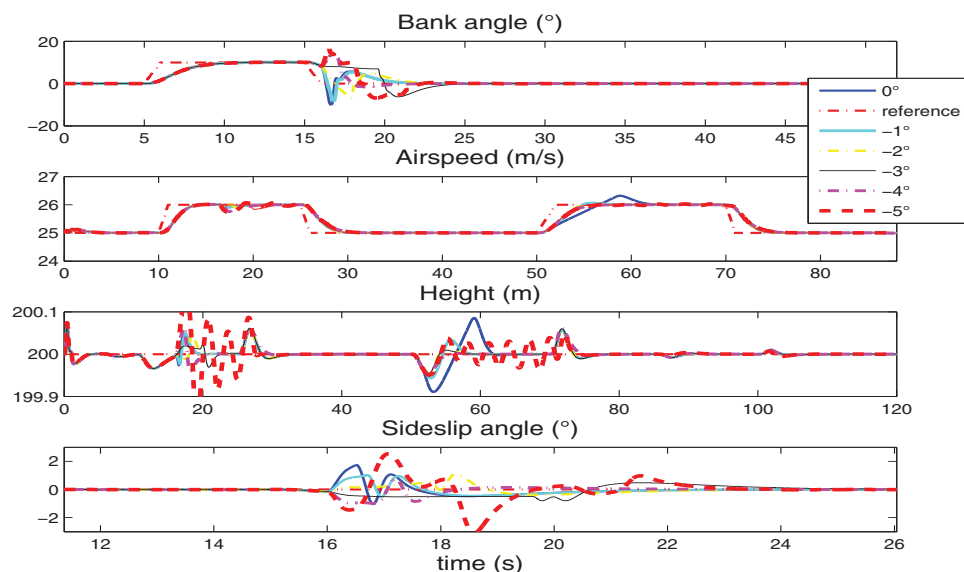Fig. 17. Right ruddervator stuck, the controls

Fig. 18. Right ruddervator stuck, the ruddervator actual position, estimation, control position and the residual

Observers has been implemented in order to detect, isolate and estimate faults. To process with the faulty ailerons, an isolation method based on a signal processing method has been presented. Future works should also take into account the redundancies provided by the right and left flaps. The fault accommodation consists in computing a new operating and a related fault-tolerant controller. For this latter, the objectives of the settings are identical to those pursued in the fault-free mode. However, the results of simulations show the importance of actuator saturations, especially in faulty mode, where to compensate for the fault, the remaining actuator strokes may be significantly reduced and may affect the control stability. Our present works deal with FTC designs which aim at setting the handling qualities while sizing the stability domain with respect to the flight envelope by considering the actuator saturations.

The first author would like to acknowledge Pr. T. Hermas for proofreading the initial manuscript.

7. References

Bateman, F., Noura, H. & Ouladsine, M. (2008a). An active fault tolerant procedure for an uav equipped with redundant control surfaces, *16th Mediterranean Conference on Control and Automation*, Ajaccio, France.

Bateman, F., Noura, H. & Ouladsine, M. (2008b). A fault tolerant control strategy for an unmanned aerial vehicle based on a sequential quadratic programming algorithm, *Conference on Decision and Control*, Cancun, Mexico.

Bateman, F., Noura, H. & Ouladsine, M. (2009). Fault tolerant control strategy for an unmanned aerial vehicle, *7th IFAC SafeProcess*, Barcelona, Spain.

Boiffier, J. (1998). *The dynamics of flight*, Wiley.

Brigaud, R. (2006). Working towards a usar stanag, *Euro UAV*, Paris, France.

Demmel, J. & Kågstrom, B. (1993). The generalized schur decomposition of an arbitrary pencil a - zb: robust software with error bounds and applications, *ACM Transaction on Mathematical Software* 19(2): 175–201.

Ducard, G. & Geering, H. (2008). Efficient nonlinear actuator fault detection and isolation for unmanned aerial vehicles, *Journal of Guidance, Control and Dynamlics* 31(1): 225–237.

Hou, M. & Patton, R. (1998). Input observability and input reconstruction, *Automatica* 34(6): 789–794.

Kobayashi, T. & Simon, D. (2003). Application of a bank of kalman filters for aircraft engine fault diagnostics, *Technical Report NASA Report 212526*, NASA.

Magni, J. F., Bennami, S. & Terlouw, J. (1997). *Robust Flight Control, a design challenge*, Springer.

MIL-HDBK-1797 (1997). U.s. military handbook mil-hdbk-1797, *Technical report*, U.S Department Of Defense.

Noura, H., Theilliol, D., Ponsart, J. & Chamsedinne, A. (2009). *Fault-tolerant Flight Control Systems*, Springer.

OSD (2003). Unmanned aerial vehicle reliability study, *Technical report*, Office of the Secretary of Defense.

Rauw, M. (1993). *A Simulink environment for flight dynamics and control analysis*, PhD thesis, Delft University of Technology, Faculty of Aerospace Engineering.

Steinberg, M. (2005). Historical review of research in reconfigurable flight control, *Journal of Aerospace Engineering* 219(4): 263–275.

Xiong, Y. & Saif, M. (2003). Unknown disturbance inputs estimation based on state functional observer design, *Automatica* 39: 1390–1398.

X.Liu, Chen, B. & Lin, Z. (2005). Linear system toolkit in matlab : structural decomposition and their applications, *Journal of Control, theory and application* 3: 287–294.

Zhang, Y. & Jiang, J. (2006). Issues on integration of fault diagnosis and reconfigurable control in active fault-tolerant control systems, *IFAC Safe Process*, Beijing, China.

Zhang, Y. & Jiang, J. (2008). Bibliographical Review on Reconfigurable Fault Tolernat Control, *Annual Reviews in Control* 32(2): pp. 229–252.

Advances in Flight Control Systems

Edited by Dr. Agneta Balint

Nonlinear problems in flight control have stimulated cooperation among engineers and scientists from a range of disciplines. Developments in computer technology allowed for numerical solutions of nonlinear control problems, while industrial recognition and applications of nonlinear mathematical models in solving technological problems is increasing. The aim of the book Advances in Flight Control Systems is to bring together reputable researchers from different countries in order to provide a comprehensive coverage of advanced and modern topics in flight control not yet reflected by other books. This product comprises 14 contributions submitted by 38 authors from 11 different countries and areas. It covers most of the currents main streams of flight control researches, ranging from adaptive flight control mechanism, fault tolerant flight control, acceleration based flight control, helicopter flight control, comparison of flight control systems and fundamentals. According to these themes the contributions are grouped in six categories, corresponding to six parts of the book.

How to reference

In order to correctly reference this scholarly work, feel free to copy and paste the following:

François Bateman, Hassan Noura and Mustapha Ouladsine (2011). Active Fault Diagnosis and Major Actuator Failure Accommodation: Application to a UAV, Advances in Flight Control Systems, Dr. Agneta Balint (Ed.), ISBN: 978-953-307-218-0, InTech, Available from: http://www.intechopen.com/books/advances-in-flight-control-systems/active-fault-diagnosis-and-major-actuator-failure-accommodation-application-to-a-uav

INTECH
open science | open minds